Huang D, DeLucia F, Corbari C, Healy N, Sazio PJA.
Numerical analysis using 2D modeling of optical fiber poled by induction.
***In: SPIE OPTO (Photonics West) Physics and Simulation of Optoelectronic Devices XXIV*. 2016, San Francisco, California, United States: Society of Photo-Optical Instrumentation Engineers.**

DOI link to article:

http://dx.doi.org/10.1117/12.2211660

Date deposited:

01/06/2017

Optical fiber poling by induction: Analysis by 2D numerical modeling

F. DE LUCIA,[1§] D. HUANG,[2§] C. CORBARI,[1] N. HEALY,[1] P.J.A. SAZIO[1,*]

[1] *Optoelectronics Research Centre, University of Southampton, SO17 1BJ, UK*
[2] *Institute of High Performance Computing, A*STAR, 1 Fusionopolis Way, 138632, Singapore*
§ These authors contributed equally to this work
**Corresponding author: pjas@soton.ac.uk*

Received XX Month XXXX; revised XX Month, XXXX; accepted XX Month XXXX; posted XX Month XXXX (Doc. ID XXXXX); published XX Month XXXX

Since their first demonstration some 25 years ago, thermally poled silica fibers have been used to realize device functions such as electro-optic modulation, switching, polarization entangled photons and optical frequency conversion with a number of advantages over bulk free-space components. We have recently developed an innovative induction poling technique that could allow for the development of complex microstructured fiber geometries for highly efficient $\chi^{(2)}$ based device applications. In order to systematically implement these more advanced poled fiber designs, we report here the development of comprehensive numerical models of the induction poling mechanism itself via 2D simulations of ion migration and space-charge region formation using finite element analysis.

OCIS codes: *(190.4370) Nonlinear optics, fibers; (230.4320) Nonlinear optical devices; (190.2620) Harmonic generation and mixing; (230.1150) All-optical devices; (000.4430) Numerical approximation and analysis.*

The development of thermal poling, a technique to generate effective second order nonlinearities in silica optical fibers [1], has found widespread applications in parametric frequency conversion [2], electro-optic modulation, switching [3] and polarization-entangled photon pair generation [4]. During thermal poling, the optical fiber is heated in order to increase the mobility of the impurity charge carriers (typically Na^+, Li^+, K^+), while a high voltage is applied for a certain time between two electrodes embedded into the fiber [5]. The static electric field due to the application of the high voltage causes the impurity charges to drift from regions at high potential towards regions at lower potential creating a space charge region located near the anode. When the sample is cooled down whilst the voltage is still applied, an electric field is frozen into the depleted region and an effective nonlinear susceptibility $\chi_{eff}^{(2)}$ is induced into the sample due to a process of third order nonlinear optical rectification. The early issues mainly related to the high risk of breakdown between the two electrodes (typically separated by a few tens of microns) were addressed by Margulis *et al.* [6], who demonstrated that it is possible to induce a value of $\chi_{eff}^{(2)}$ higher than the one obtained in the conventional case [5] by means of a poling configuration in which the two embedded electrodes are both connected to the same positive potential of the anode. The method for "charging" optical fibers has been recently further developed by De Lucia *et al.* [7], who discovered that it is possible to create a space charge region using electrostatic induction between an external inductor and the floating electrodes embedded inside a fused silica twin-hole fiber. As this novel technique avoids any physical contact to the internally embedded electrodes, it automatically lifts a number of restrictions on the use of microstructured optical fibers for poling where the multiple contacting of individual electrodes becomes a prohibitive challenge. Thus the induction poling technique, together with the use of embedded liquid electrodes such as Gallium [7], could, for example, allow for the poling of complex photonic crystal fibers (PCF), with the aim of realizing devices that fully exploit the inherently desirable PCF properties of strong optical mode confinement, dispersion, effective group index engineering, etc for highly efficient nonlinear functionality.

In order to systematically implement these advanced device concepts, it is first necessary to develop comprehensive numerical models of the induction poling mechanism itself. To this end, we report here the development of 2D simulations of induced space-charge region formation using COMSOL® finite element analysis. This builds on current numerical models by Camara et al. [8] who developed a two-dimensional analysis that accurately describes the specific geometry of poled fibers with internal electrodes, thus highlighting the role of various cations and the time evolution of second-order nonlinear profile within the fiber geometry. However, our recent experimental demonstration of electrostatic induction poling suggests that substantial modifications to the boundary conditions of these current 2D models are required in order to fully elucidate this novel poling mechanism. In the first instance, this arises due to the inherent assumption [8] that the

Commented [1]: No need for capital

outer surface of the fiber is always at ground potential. While this is a reasonable assumption when considering the experimental setup described by Margulis et al. [6], an external field applied by an inductor to floating electrodes inside fibers would, by definition, be fully shielded by this grounded surface, thus completely inhibiting the induction poling process. Furthermore, the model of Camara et al. [8] concludes that field-dependent H_3O^+ ion injection, which only becomes significant for longer poling times, does not differ significantly from constant rate injection conditions, given that the electric field at the anode-glass boundary reaches a value of $\sim 10^9$ V/m over a short time period and then remains constant. However, in the induction poling geometry, the variable floating potentials inherent in this process requires a field dependent charge injection scheme. Finally, it is also necessary to modify the field-dependency to take into account ion recombination at the cladding-air interface. We show that mapping the salient features of the induction poling experimental geometry can allow us draw a more appropriate set of boundary conditions and the modified 2D model can then be used to describe the dynamics of the second-order nonlinearity created inside the fiber when it is both close to and far away from the external inductor.

As described in [8, 9], Sodium (Na^+) is the cation of highest mobility in silica and its displacement results in a cation-depleted region of high electrical resistivity near the floating electrodes embedded inside a fused silica twin-hole fiber waveguide. The negatively charged, non-bridging oxygen sites left behind (unpaired electrons) have very low mobility at 300 °C and it is this charge separation that gives rise to the recorded field. The ions reaching the electrode-cladding surface or the air-cladding surface are assumed to recombine on these surfaces, rather than accumulate. If poling continues for long enough, the width of the depletion region increases but other slower cations are also driven into the glass (e.g. H_3O^+), which begin to neutralize the unpaired electrons. When both migration and diffusion are taken into account, the local equation of continuity and Poisson's equation leads to the following partial differential equation solved in x, y and t:

$$\frac{\partial c_i}{\partial t} + \nabla.(-D_i \nabla c_i - z_i \mu_i F c_i \nabla V) = R_i \quad \textbf{(1)}$$

where the index i represents one of the positive ionic species (i = 1 for sodium ions and i = 2 for the injected charges) and the first term in brackets accounts for diffusion and the other term corresponds to drift in the electric field. In Eq. (1), c is the concentration, D the diffusivity, z the charge, μ the ion mobility, F is Faraday's constant, V the electric potential and R the consumption or production rate. The electric field and potential distribution as a function of poling duration are derived from Maxwell's equations in the electrostatic regime, from which it is possible to deduce the second-order nonlinearity spatial distribution within the fiber.

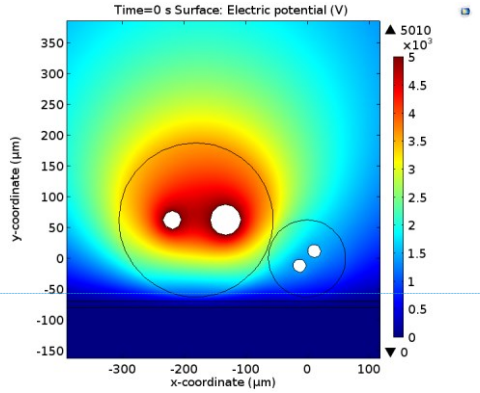

Fig. 1. 2D representation of the initial (t = 0 s) electric potential distribution developed within the electrostatic induction poling mechanism. The setup consists of the external inductor on the LHS, comprised of twin electrodes at +5kV running through a 6cm long silica fiber dielectric sheath to prevent unwanted electrical breakdown to a grounded metallic strip heater underneath. The sample being poled on the RHS is described in ref [7] and is rotated at an arbitrary angle with respect to the inductor in order to replicate realistic experimental conditions.

For the implementation of the COMSOL® model, a twin-hole fiber with dimensions identical to our experimentally relevant samples described in ref [7] (i.e. OD = 125 μm, core diameter 4.3 μm, NA = 0.17) is enclosed by a virtual "air box" in Fig. 1. An inductor placed adjacent to the fiber provides the external electric field that charges up the floating electrodes inside. The uniformly distributed Na^+ ions are assumed to have an initial concentration of 1 ppm at t = 0 s. It is also assumed that there is up to 1 ppm of H_3O^+ ions injectable at the holes, with none present within the fiber at t = 0 s. In order to achieve initial charge neutrality, negatively charged, non-bridging oxygen sites (i.e. NBO^-) with extremely low mobility are uniformly distributed inside the fiber with a concentration of 1 ppm at t = 0 s.

The holes are also assumed to be entirely filled with metal electrodes and present an equipotential. Only the outer boundaries of the "air box" (a cube with side 10cm) and the ground plane (a metallic strip heater) located 10μm underneath the inductor and fiber sample in Fig. 1 are assumed to be electrically earthed. Furthermore, H_3O^+ ions can be injected through the electrode-cladding surface when located at electric potentials higher than the surrounding cladding. An adjustable parameter σ_2 is used to describe the charge injection into the fiber [9]. We also need to consider the special case where the electric field is less than zero. In this case, H_3O^+ ions in the nearby cladding (either previously injected or diffused from other parts of the fiber) will have a negative injection rate, thus implying an outflow of H_3O^+ ions. However, if there are not any H_3O^+ ions (i.e. $c(H_3O^+) = 0$) at the electrode-cladding boundary, the injection rate will be zero even with an electric field less than zero. Therefore, the variation of the injected H_3O^+ ions density per unit of time at the electrode-cladding surface can be written as [9]:

$$\left(\frac{\partial c_2}{\partial t}\right)_{surface} = \sigma_2 E, E \geq 0 \vee E < 0 \wedge c_2 > 0 \quad \textbf{(2)}$$

Commented [2]: Should the s be here?

Commented [5]: Im using libreoffice, but something weird has happened here

Commented [6]: As shown in?

Commented [3]: These should probably be italic

Commented [4]: Comma here?

Commented [7]: space

Commented [8]: space

$$\left(\frac{\partial c_2}{\partial t}\right)_{surface} = 0, otherwise \quad (3)$$

where E is the electric field magnitude at the electrode-cladding surface.

The avalanche-like, positive feedback depletion region formation as described by Margulis *et al.* [6] in "cathode-free" fibers is also considered to operate in an enhanced form within the electrostatic induction poling mechanism [7]. However, within this configuration, it is important to note that there are two distinct and separate spatial regimes. Firstly, we can examine the evolution of the depletion region formation when the fiber sample is immediately adjacent to the external inductor as shown in Fig. 2, where the electric field from the inductor penetrates inside the fiber sample as it lacks a grounded outer surface in contrast to existing thermal poling models. As can be seen, after 100mins the electric potential distribution developed inside the fiber sample and subsequent cation migration leads to an asymmetry in comparing both the size and shape of the depletion regions formed around the internal floating electrodes. This disparity reflects the inhomogeneity of the electric field distribution close to the inductor and the strong influence of the nearby ground plane defined by the strip heater. The summation of sodium and hydronium ion depletion regions, where H_3O^+ ions occupy the negatively charged sites left by migrating sodium ions, results in a circular negative net charge distribution layer [8] surrounding the floating electrodes that will be asymmetric as detailed above.

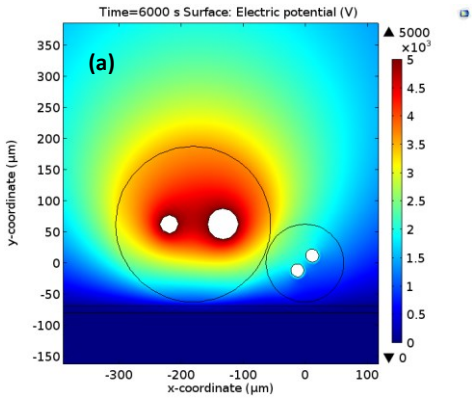

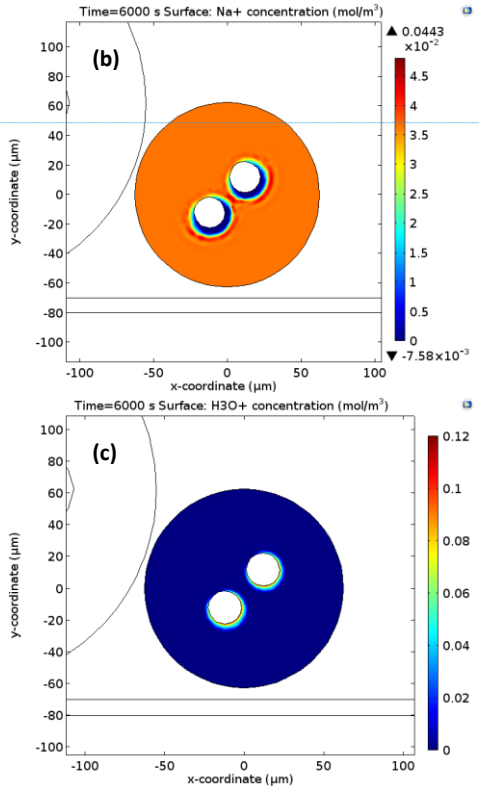

Fig. 2. Distribution of (a) electric potential, (b) Na^+ and (c) H_3O^+ mobile cations after 100 mins of poling close to the inductor.

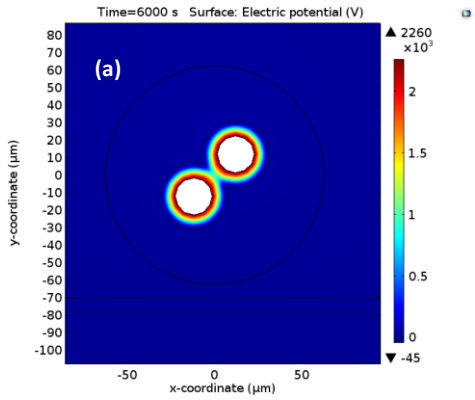

Commented [9]: Earlier et al is not itallic..

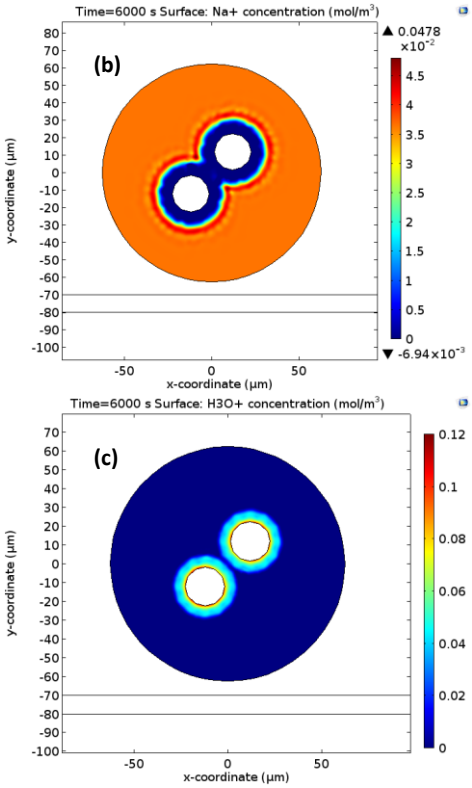

Fig. 3. Distribution of (a) electric potential, (b) Na^+ and (c) H_3O^+ mobile cations after 100 mins of poling far from the inductor.

As well as this specific behaviour close to the (6cm long) inductor, it is also possible to model the poling mechanism some distance from this region as typically the sample being poled is many times longer than the inductor itself [7]. In this spatially separated scenario it is valid to assume that the electric field due to the inductor no longer has any direct influence on the cation migration within the remainder of the sample. Nevertheless, due to the fact that during induction poling, there is very little if any, current flow through the fiber and therefore virtually no voltage drop due to metallic series resistance, the internal floating electrodes will present a well characterized equipotential surface throughout the entire sample. This means that any electric potential picked up by the floating electrodes close to the inductor will be effectively transferred to any remote location throughout the fiber. In addition, this electric potential will constantly evolve due to the temporal evolution of the induction poling dynamics. In other words, the model used to describe the induction poling mechanism far from the inductor can be considered as similar to that developed by Camara et al. [8]. Important differences remain however, such as the position of the ground potential, which rather than being the outer surface of the fiber sample, is defined instead as the outer boundaries of a virtual "air box" as well the electrically earthed metallic strip heater as shown in Fig. 4. Furthermore, the electric potential of each internal electrode is not a value fixed at t = 0 as in ref [8], but rather varies continuously as defined by the electric potential distribution close to the inductor.

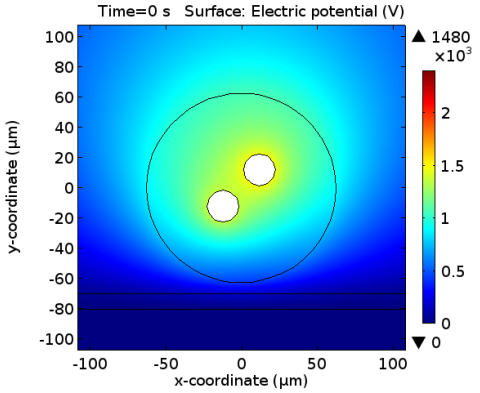

Fig. 4. Distribution of the initial (t = 0 s) electric potential far from the inductor.

It is interesting to note how the model both close to (Fig. 1) and far from (Fig. 4) the inductor exhibits a strong inhomogeneity of the electric field distribution around the floating electrodes as well as a strong influence due to the earthed strip heater. This suggests that an enhanced "avalanche-like" positive feedback [6, 7] drives the formation of the depletion region. Our simulations (question for everyone - should we include these simulations as supplementary information? We have a lot of them) also reveal that the relative azimuth rotation angle of the sample (with respect to the inductor fiber and strip heater) can further enhance the internal potential difference, demonstrating that induction poling can be engineered and optimized with many different parameters.

In summary, we have presented the results of 2D numerical simulations, developed using COMSOL Multiphysics® finite element analysis of space-charge region formation generated via electrostatic induction poling. Substantial modifications to the boundary conditions of current numerical models were required in order to fully elucidate this novel poling mechanism. This modified 2D model can be used to understand the dynamics of the second order nonlinearity created inside the fiber sample due to depletion region formation when it is both close to and far from the inductor. Our numerical analysis presents us with a powerful general method to develop models of induction poling within any complex geometry, such as for example, microstructured optical fibers that potentially allow up to four orders of magnitude improvements in second harmonic generation efficiency relative to conventionally poled step-index optical fibers [10].

Funding. EPSRC EP/I035307/1

Acknowledgment. Datasets of figures included in this paper can be found at http://dx.doi.org/10.5258/SOTON/386031

Commented [13]: I dont think this is required. Though maybe a plot of angle v PD would be nice

Commented [10]: Does this need US spelling?

Commented [11]: space

Commented [12]: Comma?

References

1. R. A. Myers, N. Mukherjee, and S. R. J. Brueck, Opt. Lett. **16**, 1732 (1991).
2. A. Canagasabey, C. Corbari, A. V. Gladyshev, F. Liegeois, S. Guillemet, Y. Hernandez, M. V. Yashkov, A. Kosolapov, E. M. Dianov, M. Ibsen, and P. G. Kazansky, Opt. Lett. **34**, 2483 (2009).
3. M. Malmstrom, O. Tarasenko and W. Margulis, Opt. Exp. **20,** 9465 (2012).
4. E. Y. Zhu, Z. Tang, L. Qian, L. G. Helt, M. Liscidini, J. E. Sipe, C. Corbari, A. Canagasabey, M. Ibsen, and P. G. Kazansky, Opt. Lett. **38**, 4397 (2013).
5. D. Wong, W. Xu, S. Fleming, M. Janos, and K-M Lo, Opt. Fib. Tech. **5**, 235 (1999).
6. W. Margulis, O. Tarasenko and N. Myrén, Opt. Exp. **17**, 15534 (2009).
7. F. De Lucia, D. Huang, C. Corbari, N. Healy and P. Sazio, Opt. Lett. **39**, 6513 (2014).
8. A. Camara, O. Tarasenko, and W. Margulis, Opt. Exp. **22**, 17700 (2014).
9. A. Kudlinski, Y. Quiquempois, and G. Martinelli, Opt. Exp. **13**, 8015 (2005).
10. T. M. Monro, V. Pruneri, N. G. R. Broderick, D. Faccio, P. G. Kazansky and D. J. Richardson, IEEE Photon. Tech. Lett. **13**, 981 (2001).

Commented [14]: Pretty sure the abbreviation is Opt. express

References

1. R. A. Myers, N. Mukherjee, and S. R. J. Brueck. “Large second-order nonlinearity in poled fused silica.” Opt. Lett., **16**, no. 22 (1991): 1732 - 1734.
2. A. Canagasabey, C. Corbari, A. V. Gladyshev, F. Liegeois, S. Guillemet, Y. Hernandez, M. V. Yashkov, A. Kosolapov, E. M. Dianov, M. Ibsen, and P. G. Kazansky. “High-average-power second-harmonic generation from periodically poled silica fibers.” Opt. Lett. **34**, no. 16 (2009): 2483-2485.
11. M. Malmstrom, O. Tarasenko and W. Margulis. “Pulse selection at 1 MHz with electrooptic fiber switch.” Opt. Exp. **20**, no. 9 (2012): 9465-9470.
12. E. Y. Zhu, Z. Tang, L. Qian, L. G. Helt, M. Liscidini, J. E. Sipe, C. Corbari, A. Canagasabey, M. Ibsen, and P. G. Kazansky. “Poled-fiber source of broadband polarization-entangled photon pairs.” Opt. Lett. **38**, no. 21 (2013): 4397-4399.
3. D. Wong, W. Xu, S. Fleming, M. Janos, and K-M Lo. “Frozen-in electrical field in thermally poled fibers”, Opt. Fib. Tech. **5** (1999): 235 – 241.
4. W. Margulis, O. Tarasenko and N. Myrén. “Who needs a cathode? Creating a second-order nonlinearity by charging glass fiber with two anodes.” Opt. Exp. **17**, no. 18 (2009): 15534 – 15540.
5. F. De Lucia, D. Huang, C. Corbari, N. Healy and P. Sazio. “Optical fiber poling by induction.” Opt. Lett. **39**, no. 22 (2014): 6513-6516.
6. A. Camara, O. Tarasenko, and W. Margulis. “Study of thermally poled fibers with a two-dimensional model.” Opt. Exp. **22**, no. 15 (2014): 17700-17715.
7. A. Kudlinski, Y. Quiquempois, and G. Martinelli. “Modeling of the $\chi^{(2)}$ susceptibility time-evolution in thermally poled fused silica. “ Opt. Exp. **13**, no. 20 (2005): 8015-8024.
8. T. M. Monro, V. Pruneri, N. G. R. Broderick, D. Faccio, P. G. Kazansky and D. J. Richardson. “Broad-Band Second-Harmonic Generation in Holey Optical Fibers.” IEEE Photon. Tech. Lett. **13**, no. 9 (2001): 981-983.